J|A|C|S ARTICLES

Published on Web 12/23/2008

Activation and Tuning of Green Fluorescent Protein Chromophore Emission by Alkyl Substituent-Mediated Crystal Packing

Jian Dong, Kyril M. Solntsev,* and Laren M. Tolbert*

School of Chemistry and Biochemistry, Georgia Institute of Technology, 901 Atlantic Drive, Atlanta, Georgia 30332-0400

Received September 3, 2008; E-mail: solntsev@gatech.edu; tolbert@chemistry.gatech.edu

Abstract: *O*-Alkyl synthetic analogues of the green fluorescent protein chromophore are nonfluorescent in solution but demonstrate a bright emission in the crystalline state. Three-dimensional steady-state and time-resolved emission spectroscopies in the solid state, as well as single-crystal X-ray diffraction, reveal the nature of complex emission in the crystals. A hypsochromic emission shift with an increase of the alkyl size is determined by the monomer-aggregate emission ratio.

Introduction

The widespread use of green fluorescent protein (GFP) as a biological marker in molecular biology, medicine, and cell biology[1−3] culminated in the 2008 Nobel Prize in chemistry. The chromophore of this protein, a *p*-hydroxybenzylideneimidazolinone (*p*-**HOBDI**), is covalently bound to the middle of an internal α-helix directed along a rigid β-barrel axis and further constrained via an extended hydrogen-bond network involving the phenolic hydroxyl and carbonyl groups, with some degree of rotational freedom.[4] Upon photoexcitation, facile excited-state proton transfer from the neutral excited chromophore occurs to form the fluorescent anionic state. However, due to the free rotation around the exo-methylene double bond in the excited state,[5] the fluorescence of either denatured protein chromophores or synthetic chromophore derivatives is tremendously quenched in fluid solution at room temperature.[6−8] Escaping constraints of the β-barrel, the cis/trans isomerization rotation exhibits a weak viscosity dependence[9−11] and can only be hindered by cooling of the solution to 77 K, resulting in fluorescence recovery. The β-barrel thus plays a critical role in providing steric hindrance to the cis/trans isomerization pathway in the excited state and allowing the superb fluorescence properties of GFP and its mutants. However, the nature of the interplay among various intermolecular forces involved in such proteins is very complex, and even as simple a question as the degree of constraint necessary to achieve high fluorescence quantum yields is still unresolved.

Previous studies have shown that the protein cavity surrounding the chromophore in GFP or GFP-like proteins in the ground state is not ideal for a planar chromophore.[5] The chromophore itself is planar because of its highly conjugated π system. The protein matrix, conversely, imposes some distortions away from planarity. This distorting force should have an effect on the fluorescence of the chromophore, for example, serving as the initial accelerant for the light-induced photocycle;[12] however, the photophysical mechanism remains unclear.

Unfortunately, most in vitro characterizations of GFP chromophores have been performed only in solution, which is different from the environment of native GFP chromophore, since β-barrel prevents the chromophore fluorescence quenching from external solvents.[1] Some gas-phase studies were reported recently.[13] Again, the deficiency of the restriction from inter-

(1) Zimmer, M. *Chem. Rev.* **2002**, *102*, 759–781.
(2) Tsien, R. Y. *Annu. Rev. Biochem.* **1998**, *67*, 509–544.
(3) *Green Fluorescent Protein: Properties, Applications, and Protocols*, 2nd ed.; Chalfie, M., Kain, S. R., Eds.; Wiley-Intersciences; Hoboken, NJ, 2005.
(4) Chen, M. C.; Lambert, C. R.; Urgitis, J. D.; Zimmer, M. *Chem. Phys.* **2001**, *270*, 157–164.
(5) Maddalo, S. L.; Zimmer, M. *Photochem. Photobiol.* **2006**, *82*, 367–372.
(6) Niwa, H.; Ionuye, S.; Horano, T.; Matsuno, T.; Kojima, S.; Kubota, M.; Ohashi, M.; Tsuji, F. I. *Proc. Natl. Acad. Sci. U.S.A.* **1996**, *93*, 13617–13622.
(7) Kojima, S.; Ohkawa, H.; Hirano, T.; Maki, S.; Niwa, H.; Ohashi, M.; Inouye, S.; Tsuji, F. I. *Tetrahedron Lett.* **1998**, *39*, 5239–5242.
(8) Litvinenko, K. L.; Webber, N. M.; Meech, S. R. *J. Phys. Chem. A* **2003**, *107*, 2616–2623.
(9) Mandal, D.; Tahara, T.; Webber, N. M.; Meech, S. R. *Chem. Phys. Lett.* **2002**, *358*, 495–501.
(10) Mandal, D.; Tahara, T.; Meech, S. R. *J. Phys. Chem. B* **2004**, *108*, 1102–1108.
(11) Litvinenko, K. L.; Webber, N. M.; Meech, S. R. *J. Phys. Chem. A* **2003**, *107*, 2616–2623.
(12) Yamada, A.; Ishikura, T.; Yamato, T. *Proteins: Struct., Funct. Bioinform.* **2004**, *55*, 1063–1069.
(13) (a) Andersen, L. H.; Bluhme, H.; Boyé, S.; Jørgensen, T. J. D.; Krogh, H.; Nielsen, I. B.; Nielsen, S. B.; Svendsen, A. *Phys. Chem. Chem. Phys.* **2004**, *6*, 2617–2627. (b) Lammich, L.; Petersen, M. Å.; Nielsen, M. B.; Andersen, L. H. *Biophys. J.* **2007**, *92*, 201–207.
(14) (a) Deans, R.; Kim, J.; Machacek, M. R.; Swager, T. M. *J. Am. Chem. Soc.* **2000**, *122*, 8565–8566. (b) An, B.-K.; Kwon, S.-K.; Jung, S.-D.; Park, S. Y. *J. Am. Chem. Soc.* **2002**, *124*, 14410–14415. (c) Luo, J.; Xie, Z.; Lam, J. W. Y.; Cheng, L.; Chen, H.; Qiu, C.; Kwok, H. S.; Zhan, X.; Liu, Y.; Zhu, D.; Tang, B. Z. *Chem. Commun.* **2001**, 1740–1741. (d) Chen, J.; Xu, B.; Ouyang, X.; Tang, B. Z.; Cao, Y. *J. Phys. Chem. A* **2004**, *108*, 7522–7526. (e) Li, Z. H.; Wong, M. S.; Tao, Y.; Lu, J. *Chem. Eur. J.* **2005**, *11*, 3285–3293.
(15) Dreuw, A.; Plöner, J.; Lorenz, L.; Wachtveitl, J.; Djanhan, J. E.; Brüning, J.; Metz, T.; Bolte, M.; Schmidt, M. U. *Angew. Chem., Int. Ed.* **2005**, *44*, 7783–7786.
(16) Ooyama, Y.; Yoshida, K. *New J. Chem.* **2005**, *29*, 1204–1212.
(17) Mizukami, S.; Houjou, H.; Sugaya, K.; Koyama, E.; Tokuhisa, H.; Sasaki, T.; Kanesato, M. *Chem. Mater.* **2005**, *17*, 50–56.

10.1021/ja806962e CCC: $40.75

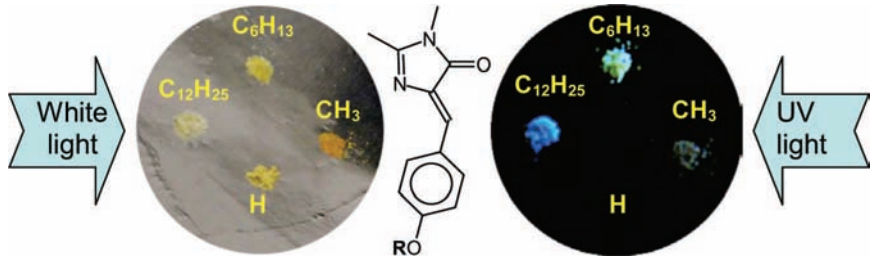

Figure 1. Real-color photograph of **ROBDI** crystals under daylight and UV illumination. The structure of **ROBDI** molecules is presented in the middle.

molecular hydrogen bonding and $\pi-\pi$ interaction limits further understanding of the chromophore in GFP and its mutants. Compared to that in solution, some fluorophore molecules can be restricted in their motions and adopt planar conformation as aggregates in the solid state, which results in more effective conjugation between the electron donor and acceptor groups of the molecules. This effective conjugation may further induce the red-shift of the emission maximum and enhance the fluorescence quantum yields.[14] However, organic fluorophores with high solid-state fluorescence are less common. Many organic chromophores are highly emissive in dilute solutions but become weakly luminescent or nonluminescent in their solid states. The formation of molecular aggregates by strong intermolecular $\pi-\pi$ interactions[15−17] or intermolecular hydrogen bonding[18] in the solid state generally results in reduction of luminescence efficiency. In view of the fact that most GFP chromophore derivatives are nonfluorescent in room-temperature solutions, it is illuminating to examine their intermolecular interactions in bulk materials that lead to the formation of aggregates, significantly altering the photophysical and photochemical properties of these molecules, resulting in large changes in their spectral characteristics and luminescence efficiency. Moreover, the optical and photophysical properties of organic π-conjugated molecules in the solid state, defined largely by their molecular packing, which in turn is controlled by various noncovalent forces, have been used as key elements in optoelectronic devices.[19,20] Understanding the nature of these forces and controlling them for the design of functional materials is of significant importance, especially with reference to tuning their application in devices such as light-emitting diodes,[21] photovoltaics,[22] and field effect transistors.[23,24] In order to provide further insight into the photophysics of this important chromophore, therefore, we embarked on a study of such chromophores in the solid state, where solid-state crystal packing might be expected to play a significant role.

Our initial results were obtained with the well-known hydroxybenzylideneimidazolinone derivative in which the protein side chains were replaced with methyl groups (**HOBDI**). Taking advantage of the well-known propensity of long-chain alkyl groups to affect aggregation states in solution and packing in the solid, we also prepared and obtained the fluorescence properties of several isoelectronic *O*-alkyl benzylideneimidazolinone (**ROBDI**) GFP chromophore derivatives in solution and in the solid state. The role of crystal packing in controlling the intensity and wavelength of the solid-state fluorescence of these derivatives is elucidated, and its relevance to GFP itself is described.

Results

Photophysical Properties in Solution. The synthesis and purification of alkoxybenzylideneimidazolinones (**ROBDI**) derivatives (R = C_6H_{13} ("Hex"), $C_{12}H_{25}$ ("Ddec")) were analogous to those of the **MeOBDI** reported by us earlier[25] and are described in the Supporting Information. The absorption spectra of all neutral **ROBDI** derivatives were measured in various solvents. As in previous measurements of **MeOBDI**,[25] the absorption maxima of these derivatives (ca. 370 nm) were nearly identical and exhibited the weak solvent dependence reported earlier. Similar to **HOBDI**, all **ROBDI** derivatives exhibited an extremely weak steady-state emission in various solvents at room temperature,[26] which was obscured by Raman scattering. The λ_{max} values observed for these derivatives (~450 nm) were also consistent with those previously reported.[26,27]

Solid-State Luminescence. In contrast to solutions, the crystals of **HexOBDI** and **DdecOBDI** exhibited strong greenish-yellow and blue fluorescence emission, respectively, upon irradiation with a hand-held UV lamp, whereas **MeOBDI** exhibited weaker dark-red fluorescence (see Figure 1). The crystals of **HOBDI**, however, still remained nonfluorescent.

(18) Yoshida, K.; Uwada, K.; Kumaoka, H.; Bu, L.; Watanabe, S. *Chem. Lett.* **2001**, *8*, 808–809.
(19) Kumar, N. S. S.; Varghese, S.; Rath, N. P.; Das, S. *J. Phys. Chem. C.* **2008**, *112*, 8429–8437.
(20) (a) Hudson, A. J.; Weaver, M. S. In *Functional Organic and Polymeric Materials*; Richardson, T. H., Ed.; John Wiley & Sons: New York, 2000. (b) Kaneko, M. In *Handbook of Organic Molecules and Polymers*; Nalwa, H. S., Ed.; Wiley: New York, 1997.
(21) (a) Burroughes, J. H.; Bradley, D. D. C.; Brown, A. R.; Marks, R. N.; Mackay, K.; Friend, R. H.; Holmes, P. L.; Holmes, A. B. *Nature* **1990**, *347*, 539–541. (b) Kraft, A.; Reichert, A. *Tetrahedron* **1999**, *55*, 3923–3930. (c) *Organic Light Emitting Devices: Synthesis, Properties and Applications*; Müllen, K., Scherf, U., Eds.; Wiley-VCH: Weinheim, 2006. (d) Yamaguchi, Y.; Ochi, T.; Miyamura, S.; Tanaka, T.; Kobayashi, S.; Wakamiya, T.; Matsubara, Y.; Yoshida, Z.-I. *J. Am. Chem. Soc.* **2006**, *128*, 4504–4505. (e) Armaroli, N.; Accorsi, G.; Holler, M.; Moudam, O.; Nierengarten, J.-F.; Zhou, Z.; Wegh, R. T.; Welter, R. *Adv. Mater.* **2006**, *18*, 1313–1316.
(22) (a) O'Neill, M.; Kelly, S. M. *Adv. Mater.* **2003**, *15*, 1135–1146. (b) Shirota, Y. *J. Mater. Chem.* **2005**, *15*, 75–93. (c) Strohriegl, P.; Grazulevicius, J. V. *Adv. Mater.* **2002**, *14*, 1439–1452.
(23) (a) Dimitrakopoulos, C. D.; Malenfant, P. R. L. *Adv. Mater.* **2002**, *14*, 99–117. (b) Garnier, F.; Hajlaoui, R.; Yassar, A.; Srivastava, P. *Science* **1994**, *265*, 1684–1686. (c) Li, X.-C.; Sirringhaus, H.; Garnier, F.; Holmes, A. B.; Moratti, S. C.; Feeder, N.; Clegg, W.; Teat, S. J.; Friend, R. H. *J. Am. Chem. Soc.* **1998**, *120*, 2206–2207. (d) Kelly, S. M.; O'Neill, M. In *Handbook of Advanced Electronic and Photonic Materials*; Nalwa, H. S., Ed.; Academic Press: San Diego, CA, 2000; Vol. 1,Chapter 1.
(24) Davis, R.; Kummar, N. S. S.; Abraham, S.; Suresh, C. H.; Rath, N. P.; Tamaoki, N.; Das, S. *J. Phys. Chem. C* **2008**, *112*, 2137–2146.
(25) Dong, J.; Solntsev, K. M.; Tolbert, L. M. *J. Am. Chem. Soc.* **2006**, *128*, 12038–12039.
(26) Solntsev, K. M.; Poizat, O.; Dong, J.; Rehault, J.; Lou, Y.; Burda, C.; Tolbert, L. M. *J. Phys. Chem. B* **2008**, *112*, 2700–2711.
(27) Kummer, A. D.; Kompa, C.; Niwa, H.; Hirano, T.; Kojima, S.; Michel-Beyerle, M. E. *J. Phys. Chem. B* **2002**, *106*, 7554–7559.

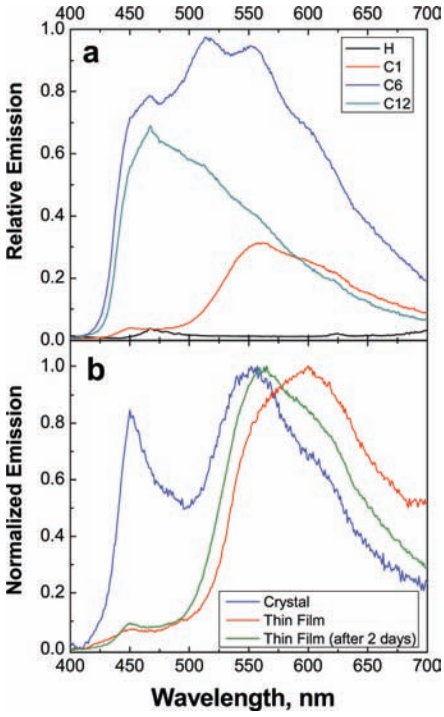

Figure 2. (Top) Solid-state fluorescence spectra of **HOBDI** (crystal) and **MeO-DdecOBDI** (thin films). (Bottom) Normalized solid-state fluorescence spectra of **MeOBDI**; $\lambda_{ex} = 370$ nm.

In order to investigate the difference in the solid-state photophysical properties among these **ROBDI** derivatives, we measured the fluorescence excitation and emission spectra of the crystals and thin films. With the exception of **MeOBDI**, the emission spectra in their powdered crystalline state and in thin films formed from their melts were almost identical. Considering the lack of reproducibility of the fluorescence intensity in loading powdered crystalline samples,[28,29] thin films of these **ROBDI** derivatives were used in the measurements. A thin-film form was not available for **HOBDI**, because it decomposed above 200 °C. The fluorescence spectra of these **ROBDI** derivatives were much broader, and their emission intensities were significantly higher, compared to those in solution. As shown in Figure 2, the fluorescence intensity of **HOBDI** was still low and showed a very weak emission peak at about 465 nm. Compared to **HOBDI**, more than a 10-fold fluorescence enhancement was observed for its alkyl ethers. The emission maximum of a **DdecOBDI** thin film sample was also at ~465 nm, with a peak position similar to that of the solid-state **HOBDI** sample; however, the spectrum of **MeOBDI** was red-shifted to $\lambda_{max} = 560$ nm. The **HexOBDI** sample showed the broadest and highest fluorescence intensity and appeared as a superposition of the **MeOBDI** and **DdecOBDI** emission bands.

The optical properties of **MeOBDI** samples depended significantly on the nature of their preparation (Figure 2, bottom). The emission spectra of its crystals showed two structured bands, with one sharp peak at 450 nm and the other broad band centered at ~550 nm. The emission spectra of thin films formed by heating above its melting point and rapidly cooling to room temperature showed a band centered at ~600 nm. However, this kind of thin film was less stable thermally, and a blue-shift in its emission maximum was observed after 2 days at room temperature. The

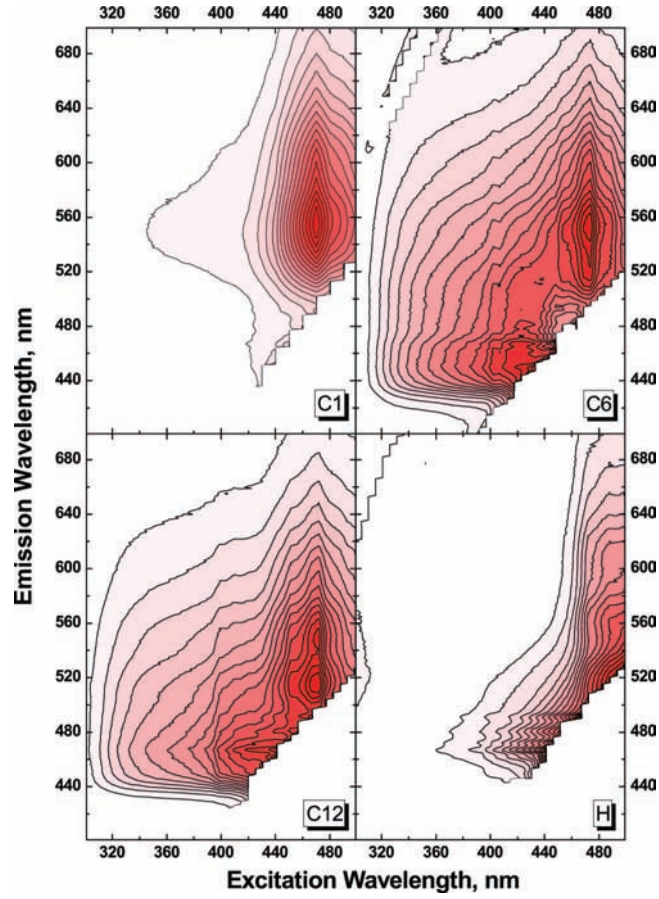

Figure 3. Excitation−emission contour plots of solid **ROBDI** samples. The difference between the neighboring lines corresponds to the constant intensity difference on a linear scale. Deeper colors correspond to higher intensities.

difference in fluorescence of two different solid states could be attributed to the formation of a thermodynamically unstable aggregation form upon melting and rapid cooling. A similar polymorphic phenomenon was also reported in ref 19. In contrast, slowly cooled thin films were very stable at ambient conditions. In addition, the fluorescence of crystalline **MeOBDI**, as well as **HexOBDI** and **DdecOBDI**, vanished above its melting point (Figure S1, Supporting Information), but the fluorescence reappeared after cooling. This process was reversible. In contrast to the crystals of the Photoactive Yellow Protein synthetic chromophore[30] no fluorescence turn-off or turn-on was observed upon prolonged irradiation of the **ROBDI** crystals, demonstrating an absence of photoinduced cis−trans isomerization.

For a more detailed study of the photophysical properties of these **ROBDI** derivatives in the solid phase, we investigated their excitation−emission matrix (EEM) spectroscopy. EEM spectroscopy has recently emerged as an effective method for spectroscopic characterization of multifluorophoric systems.[31−34] We collected the emission spectra of the fluorophores at room temperature, scanning the excitation wavelength from 250 to

(28) Ramachander, R.; Jiang, Y.; Li, C.; Eris, T.; Young, M.; Dimitrova, M.; Narhi, L. *Anal. Biochem.* **2008**, *376*, 173–182.
(29) Gardecki, J. A.; Maroncelli, M. *Appl. Spectrosc.* **1998**, *52*, 1179–1189.
(30) Usman, A.; Masuhara, H.; Asahi, T. *J. Phys. Chem. B* **2006**, *110*, 20085–20088.
(31) Weber, G. *Nature* **1961**, *190*, 27–29.
(32) Clower, C.; Solntsev, K. M.; Kowalik, J.; Tolbert, L. M.; Huppert, D. *J. Phys. Chem. A* **2002**, *106*, 3114–3122.
(33) Gill, D. M.; Wright, J. C.; McCaughan, L. *Appl. Phys. Lett.* **1994**, *64*, 2483–2485.
(34) Divya, O.; Mishra, A. K. *Anal. Chim. Acta* **2007**, *592*, 82–90.

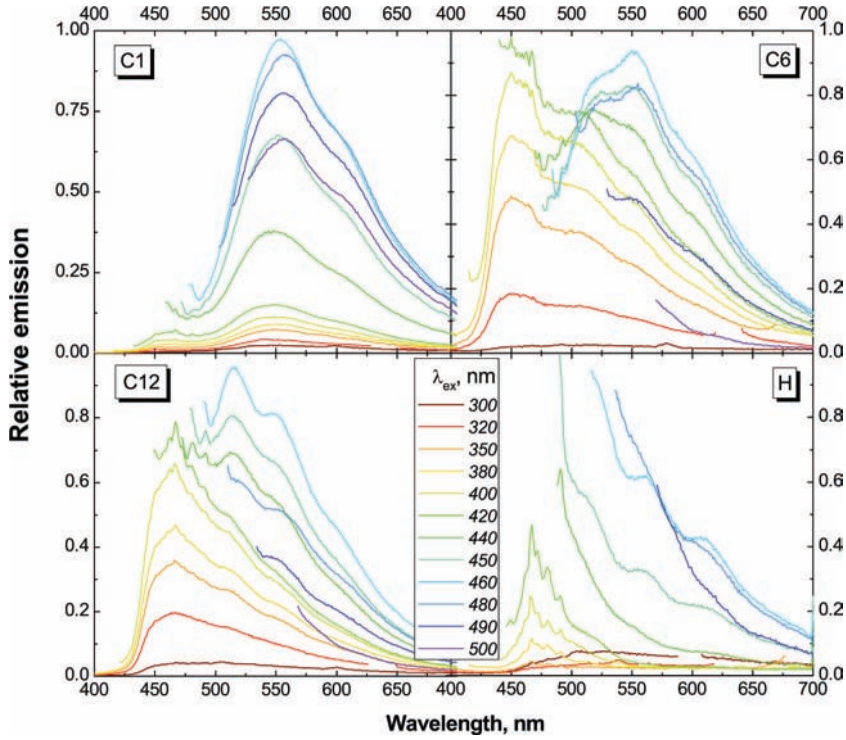

Figure 4. Emission spectra of solid **ROBDI** samples at various excitation wavelengths. Color coding is the same for all graphs.

550 nm at 5 nm increments. In Figure 3, the emission spectra of the **ROBDI** samples are displayed as contour plots, which allowed the observation of every emission band and its correlation to the appropriate excitation wavelength. The contour plot of **MeOBDI** was the simplest, showing mainly only one symmetric peak at E_x/E_m of 470/550 nm. The contour plots of **HexOBDI** and **DdecOBDI** were highly asymmetrical, demonstrating two major emissive species: a long-wavelength one similar to that of **MeOBDI** with E_x/E_m peaks of 470/550 nm for **HexOBDI** and 470/515 nm for **DdecOBDI**, and another at shorter wavelengths with E_x/E_m peaks of 420/460 nm for **HexOBDI** and 440/460 nm for **DdecOBDI**. Some emission was observed from **HOBDI** only upon long-wavelength visible excitation, but not with UV light (Figures 1 and 3). Manual deletion of the strong excitation light scattering signals resulted in the empty zones in the bottom right corner of each graph. It should be noted that the light scattering, as well as refraction from crystal or film morphology and geometrical effects observed on microspectrophotometer devices, may slightly alter the fluorescence spectra. Some selected emission spectra from each sample demonstrating the spectral evolution upon excitation wavelength shifts are presented in Figure 4.

Lifetime measurements used in fluorescence spectroscopy, for instance, time-correlated single-photon counting (TCSPC), are expected to be less dependent on concentration and method of preparation than steady state, thus providing an easier comparison of crystalline samples. A combination of time-resolved and steady-state emission techniques may allow the deconvolution of contributions from multichromophoric systems. Fluorescence lifetimes obtained from measurements of the solid-state of materials are often complex, and multiexponential decay profiles are observed, which could be attributed to the presence of molecules in different states of aggregation in the solid state.[35] In addition, due to the complexity of the excitation spectra in the solid-state **ROBDI** derivatives, it is feasible to use pulsed diode lasers with two different wavelengths (372 and 467 nm) as excitation sources in the TCSPC system. To reveal the complex nature of the emitting species in the solid-state samples, we collected intensity−wavelength−time 3D surfaces similarly to the steady-state results.

Figure 5 demonstrates the decay surfaces of alkoxyBDIs. At 372 nm excitation, the surfaces of all compounds clearly demonstrate an existence of two major decaying species: a short-decaying one with a maximum around 450 nm, and another significantly longer, decaying with the maximum around 570 nm therefore resembling steady-state results. The relative amplitude of the short-lived component increased dramatically in the order of C1 > C6 > C12. The **HOBDI** emission at 372 nm excitation was too weak and short-lived to be detected with our TCSPC instrument. The time-resolved emission surfaces of all compounds at 467 nm excitation demonstrated only one component with the emission maximum at 570 nm observed in the previous case. The decays of this component were uniform through the whole spectrum for each compound. Some selected 2D fluorescence decay curves are presented in Figure 6. One can see that the nonexponential decay at 570 nm for each sample was practically independent of the excitation wavelength. The average lifetime of the former was higher for the long-chain derivatives. The decay at 450 nm was ultrashort for **MeOBDI** and much longer for **HexOBDI** and **DdecOBDI**. The data measured on the 10 or 20 ns time scales were fitted to a sum of two or three ($n = 2$ or 3) exponentials,

$$\frac{I(t)}{I(0)} = \sum_{i=1}^{n} A_i \exp(-t/\tau_i) \otimes \mathrm{IRF}(t) \qquad (1)$$

and convoluted with the instrument response function (IRF). It was normalized so that $\sum_{i=1}^{n} A_i = 1$. The results of fitting are presented in Table 1.

(35) Li, H.; He, L.; Zhong, B.; Li, Y.; Wu, S.; Liu, J.; Yang, G. *ChemPhysChem.* **2004**, *5*, 124–127.

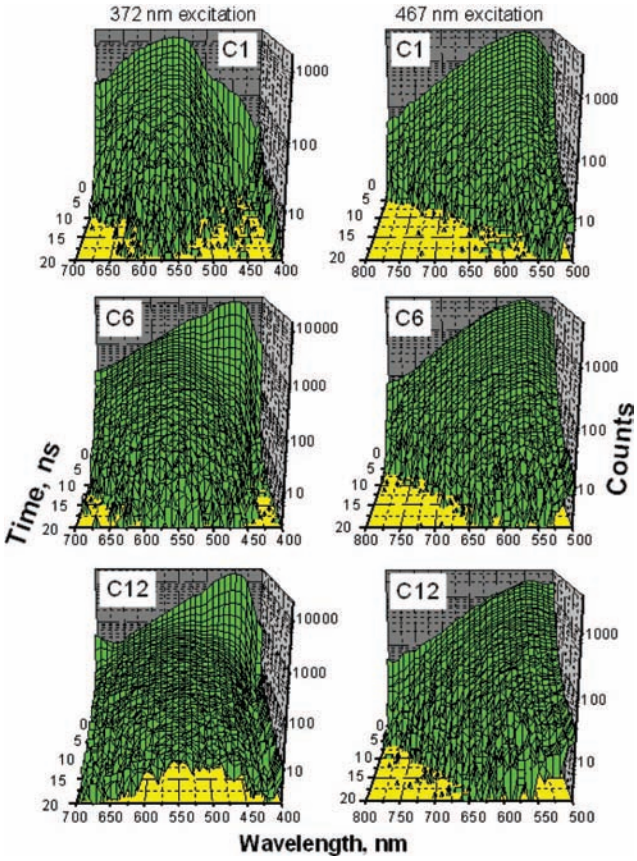

Figure 5. Time-resolved emission spectra of solid **ROBDI** samples at 372 and 467 nm laser excitation.

Crystal Structure. Single crystals of all **ROBDI** compounds were grown at room temperature in dichloromethane or ethyl acetate solvents. Their crystal data are summarized in Table 2.

HOBDI has eight molecules per unit cell (Figure S2, Supporting Information), with the molecules arranged into two nonequivalent stacks with their dipoles pointing in opposite directions in a herringbone fashion.[36] A part of the X-ray structure of **HOBDI** containing four monomer molecules is shown in Figure 7a. The figure also includes two major alignments of the molecules, namely, (1) AB (alternate stack) and (2) AA′ (neighboring stack), which are separately shown in Figure 7b,c. Most significantly, an intermolecular hydrogen bond between the hydroxyl proton and the carbonyl oxygen (O−H···O distance and angle are 2.673 Å and 173.7°, respectively) is observed in AB couples of **HOBDI**. The hydrogen-bond formation is accompanied by the C═O bond lengthening in **HOBDI** as compared to all other **ROBDIs** (see Table 2). In addition, the imidazolinone and phenyl moieties in AA′ and BB′ couples overlap, with interplane distances of 3.590 and 3.546 Å. Intermolecular hydrogen bonding[18] and $\pi-\pi$ interactions in the solid state[15,16,37] have been reported as general factors in fluorescence quenching.

One unit cell of **MeOBDI** contains four molecules (Figure S3, Supporting Information). The structure of **MeOBDI** is similar to **HOBDI**, but the angle between two mean planes of alternate molecules increases from 31.9° to 50.4° (see Figure 8a). Since the hydroxyl proton is replaced by a methyl group in **MeOBDI**, the possibility of an inter- or intramolecular hydrogen bond is eliminated. Moreover, this herringbone configuration is stabilized in the AB couple by aromatic C−H···O (2.651 Å) and aromatic C−H···N (2.845 Å) interactions,[24] as shown in Figure 8b. In the case of AA′ (not shown), aromatic $\pi-\pi$ interactions from the phenyl rings of both A and A′ are seen, and the overlapping of the parallel layers is partially reduced compared to that in **HOBDI**. The dipole moments of the molecules in the AA′ pair are still antiparallel as for **HOBDI**.

The structure of **HexOBDI** is significantly different from those of **HOBDI** and **MeOBDI**. It has only two molecules per unit cell (Figure S4, Supporting Information). The relative alignment of A and B is the most altered, as they are aligned antiparallel to each other (Figure 9a), while in both **HOBDI** and **MeOBDI** they are arranged in an angular fashion with respect to each other. Two strong intermolecular aromatic C−H···O (2.677 Å) interactions (electronically) are responsible for the planar AB alignment, whereas the AA′ unit is characterized by the presence of both aliphatic C−H···O and aliphatic C−H···π interactions (Figure 9b). Such C−H···O hydrogen-bonding-stabilized planarization of crystal structures has been reported for various molecules.[24,38] The only aggregation interaction that can be observed consists of aromatic C−H and imidazoline moiety interactions with a distance of 3.298 Å between neighboring molecules. However, since A and A′ are translated along both the long and short axes relative to each other with parallel dipole moments, the π-overlap between them is also minimized (Figure 9c).

The structure of **DdecOBDI** is very similar to that of **HexOBDI,** with AB- and AA′-type dimer units with aromatic C−H···O, aliphatic C−H···O, and aliphatic C−H···π interactions (Figures S5,Supporting Information; Figure 10). Compared to **HexOBDI**, the A and B units of **DdecOBDI** make a stronger interaction for the coplanar alignment while the aromatic planes of the shifted parallel units A and A′ in **DdecOBDI** are located at a larger distance compared to **HexOBDI** (see Figures 9b,c and 10b,c).

Discussion

The GFP synthetic chromophore **HOBDI** and its derivatives are nonfluorescent in solutions at room temperature, and their fluorescence quenching is caused presumably by a nonadiabatic transition induced by the free rotation around the exo-methylene double bond in the excited state. In their solid states, the formation of aggregates from intermolecular interaction significantly alters the photophysical and photochemical properties of the molecules, resulting in large changes in their spectral characteristics and luminescence efficiency.[39−41]

The most striking difference among the solid-state fluorescence data is the quenching of the **HOBDI** fluorescence. The crystal packing of **HOBDI** indicates the electronic interaction is maximum for AA′, BB′ couples; in addition, the effect of an

(36) (a) Koren, A. B.; Curtis, M. D.; Francis, A. H.; Kampf, J. W. *J. Am. Chem. Soc.* **2003**, *125*, 5040–5050. (b) Gierschner, J.; Ehni, M.; Egelhaaf, H.-J.; Medina, B. M.; Beljonne, D.; Benmansour, H.; Bazan, G. C. *J. Chem. Phys.* **2005**, *123*, 144914. (c) Spano, F. C. *J. Chem. Phys.* **2003**, *118*, 981. (d) Nishio, M. *CrystEngComm* **2004**, *6*, 130–158.

(37) Mizukami, S.; Houjou, H.; Sugaya, K.; Koyama, E.; Tokuhisa, H.; Sasaki, T.; Kanesato, M. *Chem. Mater.* **2005**, *17*, 50–56.

(38) (a) Desiraju, G. R. *Acc. Chem. Res.* **1996**, *29*, 441–449. (b) Desiraju, G. R. *Acc. Chem. Res.* **2002**, *35*, 565–573. (c) Vargas, R.; Garza, J.; Dixon, D. A.; Hay, B. P. *J. Am. Chem. Soc.* **2000**, *122*, 4750–4755. (d) Jeffrey, G. A. *An Introdution to Hydrogen Bonding*; University Press: Oxford, U.K., 1997.

(39) Cornil, J.; Beljonne, D.; Calbert, J.-P.; Brédas, J.-L. *Adv. Mater.* **2001**, *13*, 1053–1067.

(40) Vaday, S.; Geiger, H. C.; Cleary, B.; Perlstein, J.; Whitten, D. G. *J. Phys. Chem. B* **1997**, *101*, 321–329.

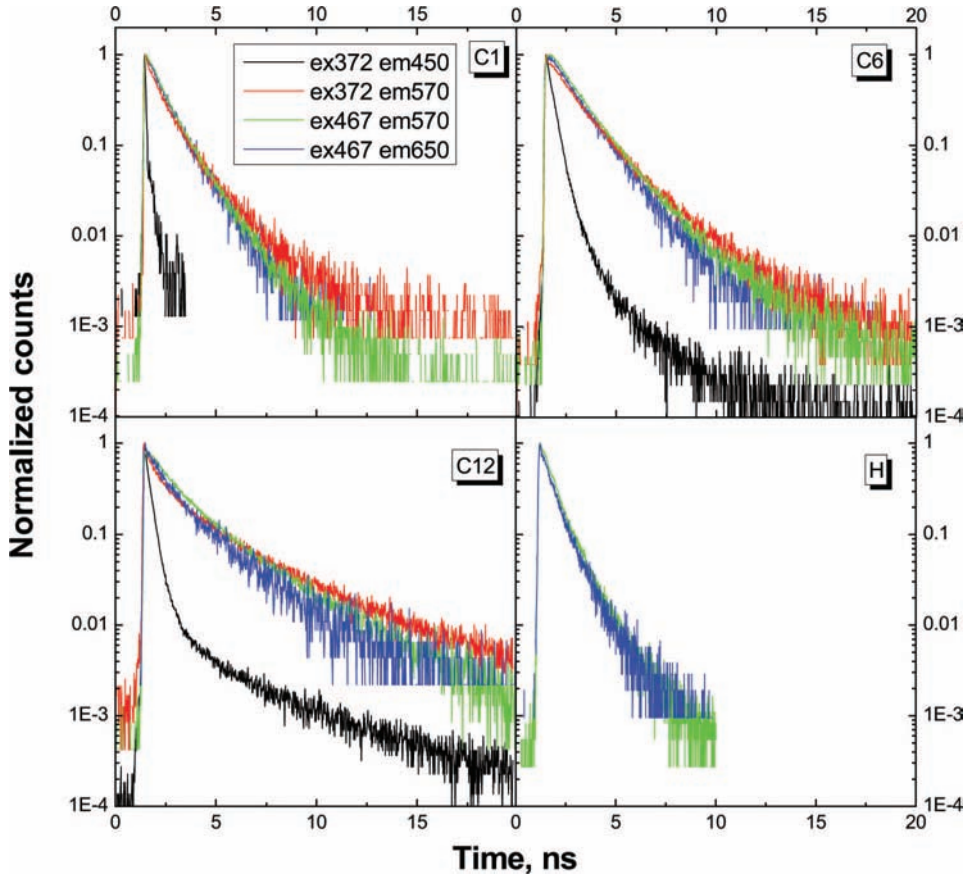

Figure 6. Fluorescence decays curves of solid **ROBDI** samples at various excitation wavelengths detected at various emission wavelengths. Color coding is the same for all graphs.

Table 1. Parameters Obtained from Multi-exponential Fits (Eq 1) of the **ROBDI** Time-Resolved Emission Data[a]

compound	λ_{obs}, nm	τ_1, ns	A_1/A_i	τ_2, ns	A_2/A_i	τ_3, ns
MeOBDI	450	0.020[b]	0.99	0.72	0.01	–
	570	0.04	0.52	0.54	0.30	1.6
HexOBDI	450	0.12	0.49	0.34	0.49	1.2
	570	0.09	0.34	1.2	0.51	2.6
DdecOBDI	450	0.11	0.76	0.36	0.23	3.7
	570	0.11	0.59	0.88	0.25	3.4
HOBDI	570	0.03	0.65	0.38	0.22	0.98

[a] C1−C12 samples were excited at 372 nm. HO sample was excited at 467 nm. The quality of fit was evaluated by the residuals analysis and χ^2 values, which were always smaller than 1.15. [b] Below the resolution of our TCSPC system.

intermolecular hydrogen bond may lead to the efficient quenching of the **HOBDI** solid-state fluorescence. This is in contrast to the fluorescent proteins, where the presence of a hydrogen-bonding arginine (R96) is an obligatory component of maturation.[42] The spectroscopic role of R96 has not been successfully explained, and we suspect that, in the absence of R96 (pK_a = 12.48 in water), other hydrogen-bonding residues may lead to formal proton transfer in the excited state, leading to fluorescence quenching just as in the **HOBDI** crystal. Strong hydrogen bonding involving both hydroxyl and carbonyl groups, leading to quenching, may have interesting analogies with other proteins having hydrogen bonds of similar nature. We have also recently demonstrated[26] that in *meta*-**HOBDI** the excited-state proton transfer (ESPT) is diabatic and induces the $S_1 \rightarrow S_0$ deactivation when it leads to a zwitterion (protonation of the *m*-**HOBDI** anion, deprotonation of the *m*-**HOBDI** cation), but it is adiabatic when it leads to a single-charged form (deprotonation of *m*-**HOBDI** and *m*-**MeOBDI**). This behavior agrees perfectly with the previous assumption about the role of zwitterion as a quenching product in the GFPs.[43]

In contrast to **HOBDI**, the solid-state luminescence of alkyl **ROBDI** derivatives is enhanced dramatically compared to that observed in solution, which may be attributed to "freezing" of planar conformation of the fluorophores, resulting in more effective conjugation between the electron donor and acceptor groups and avoiding the quenching present in hydrogen bonding crystals. However, such enhancement is not uniform, and we conclude that freezing of conformation is a necessary but not sufficient condition for efficient emission. Various emission colors were observed from **ROBDI** crystals upon UV irradiation, which was a little surprising since the electronic structures of the chromophores were essentially the same. We will discuss now how the inert alkyl groups play a dramatic role in color tuning of the **ROBDI** crystals emission.

Consistent with previous reports,[24,44] the solid-state fluorescence spectrum of the derivative possessing a shorter alkoxy

(41) (a) Sheikh-Ali, B. M.; Rapta, M.; Jameson, G. B.; Cui, C.; Weiss, R. G. *J. Phys. Chem.* **1994**, *98*, 10412–10418. (b) Sheikh-Ali, B. M.; Weiss, R. G. *J. Am. Chem. Soc.* **1994**, *116*, 6111–6120. (c) Lewis, F. D.; Yang, J.-S.; Stern, C. L. *J. Am. Chem. Soc.* **1996**, *118*, 2772–2773. (d) Lewis, F. D.; Yang, J.-S.; Stern, C. L. *J. Am. Chem. Soc.* **1996**, *118*, 12029–12037.

(42) Wood, T. I.; Barondeay, D. P.; Hitomi, C.; Kassmann, C. J.; Tainer, J. A.; Getzoff, E. D. *Biochemistry* **2005**, *44*, 16211–16220.

(43) Weber, W.; Helms, V.; McCammon, J. A.; Langhoff, P. W. *Proc. Natl. Acad. Sci. U.S.A.* **1999**, *96*, 6177–6182.

Table 2. Summary of Crystallographic Data for **ROBDI** derivatives

	HOBDI	MeOBDI	HexOBDI	DdecOBDI
empirical formula	$C_{12}H_{12}N_2O_2$	$C_{13}H_{14}N_2O_2$	$C_{18}H_{24}N_2O_2$	$C_{24}H_{36}N_2O_2$
formula weight	216.24	230.26	300.39	384.55
crystal system	monoclinic	monoclinic	triclinic	triclinic
space group	$P2(1)/n$	$P2(1)/n$	$P\bar{1}$	$P\bar{1}$
Z	8	4	2	2
a, Å	7.6165(3)	11.4832(4)	7.4623(5)	7.4678(3)
b, Å	16.5619(7)	7.7162(3)	10.0972(6)	10.2078(7)
c, Å	16.8917(5)	13.3246(5)	11.7537(8)	15.4909(7)
α, deg	90	90	88.216(3)	85.971(3)
β, deg	92.805(1)	102.553(2)	79.002(2)	85.619(4)
γ, deg	90	90	71.188(2)	71.602(4)
V, A^3	2128.23(15)	1152.43(7)	822.48(9)	1115.91(10)
d_{calc}, Mg/cm^3	1.350	1.327	1.213	1.144
μ, mm^{-1}	0.767	0.740	0.629	0.562
total reflections	7768	7792	5807	5685
unique reflections	3176	1863	2247	3090
R_{int}	0.0130	0.0246	0.0173	0.0244
final R indices, R1, wR2	0.0338, 0.0899	0.0361, 0.0997	0.0353, 0.1029	0.0449, 0.1261
R indices (all data), R1, wR2	0.0349, 0.0908	0.0384, 0.1015	0.0396, 0.1077	0.0557, 0.1349
phenyl−imidazole interplanar angle, deg	7.2	3.4	5.5	4.7
C═O distance, Å	1.235	1.222	1.217	1.218

group (**MeOBDI**) is significantly broader and red-shifted compared to that of the derivative with longer alkoxy chains (**DdecOBDI**), while the solid-state intensive emission band of **HexOBDI** is in between and apparently possesses peaks from both solid-state derivatives. The red-shifted emission observed in the solid state is clearly different from that in solution, because the absorption and emission spectra are almost independent of the length of the alkoxy substituent in the latter case. Solid-state EEM spectra of **MeOBDI** clearly show a totally different E_x/E_m peak than that in solution. The significant red-shift in the emission spectrum is presumably due to electronic coupling resulting from aggregation of molecules, a widely reported phenomenon.[24,39,41,44] The studies on the dependence of the emission spectra upon dilution with an inert material have shown that the formation of red-shifted band is due to the formation of aggregates and is not merely due to planarization. Moreover, the fluorescence spectrum of the thin films of **MeOBDI** formed by rapid cooling is more red-shifted, broader, and unstructured, indicating strong intermolecular vibronic coupling. Similar reports[19] suggest the existence of the alternate molecular packing changing from a herringbone-type arrangement in the powdered crystalline state to a brickstone-type arrangement in thin-film form. In the brickstone arrangement, the material would result in a significant enhancement of the overlap of the π orbitals of

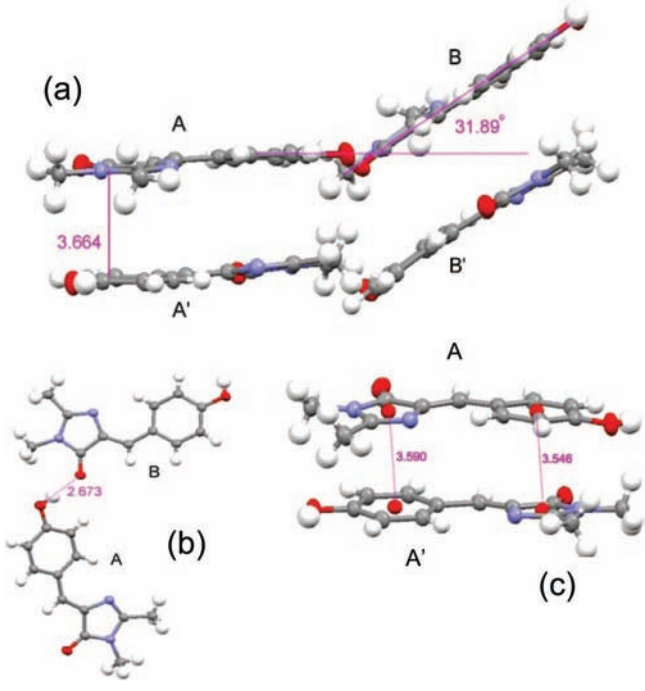

Figure 7. (a) Tetramer unit of **HOBDI** taken from the X-ray structure. (b,c) Dimer units showing the AB and AA′ interaction. On this and the following figures, all distances are in angstrom units.

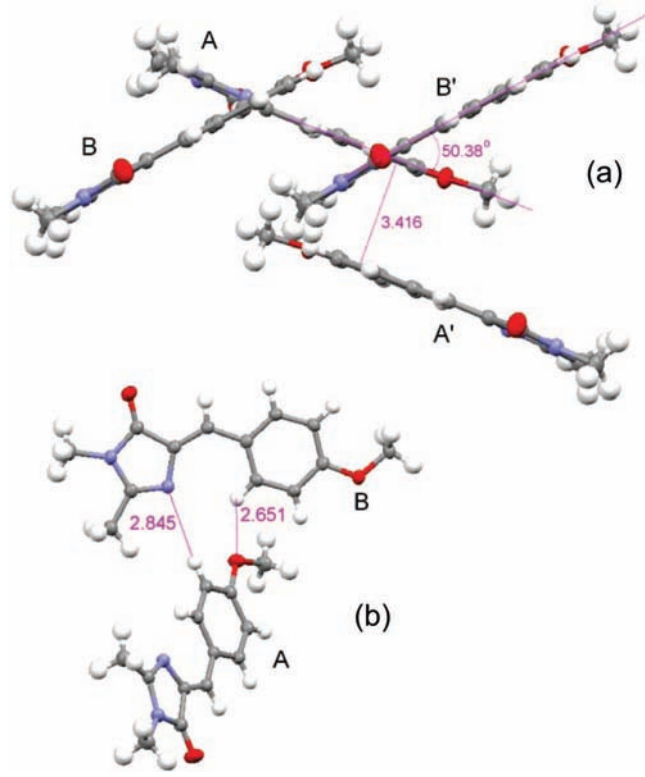

Figure 8. (a) Tetramer unit of **MeOBDI** taken from the X-ray structure. (b) Dimer unit showing the AB interaction.

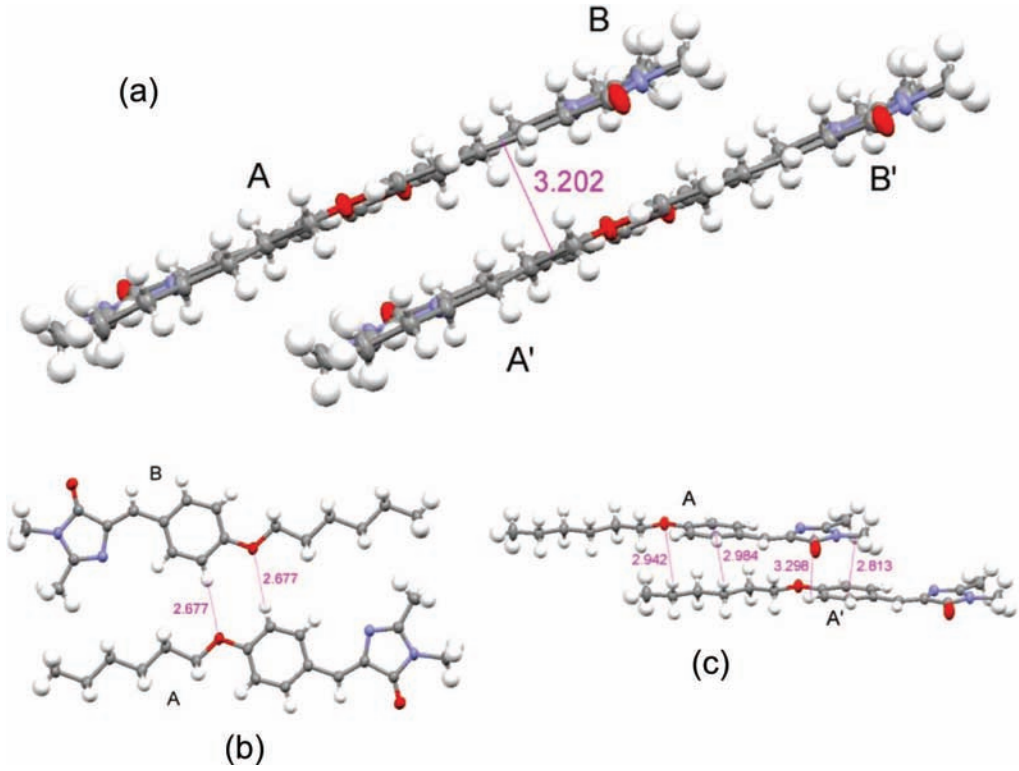

Figure 9. (a) Tetramer unit of **HexOBDI** taken from the X-ray structure. (b,c) Dimer units showing the AB and AA′ interactions.

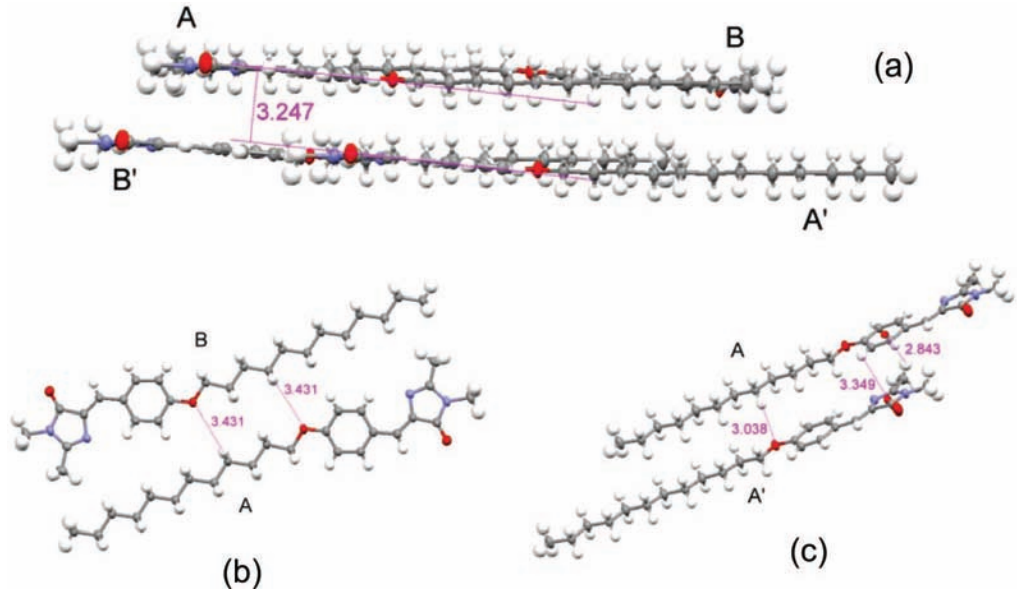

Figure 10. (a) Tetramer unit of **DdecOBDI** taken from the X-ray structure. (b,c) Dimer units showing the AB and AA′ interaction.

the molecules from alternate stacks, leading to significant increase in electronic coupling between these molecules and red-shifted emission. A significant number of publications demonstrate a dramatic role for $\pi-\pi$ stacking between the chromophore and the neighboring aromatic amino acid,[45] resulting in the important bathochromic emission shift of the emission, as a consequence producing the whole family of yellow fluorescent proteins.[2,3,46]

In the case of **HexOBDI** and **DdecOBDI**, an additional E_x/E_m peak at 420/460 nm, which is only ~25 nm red-shifted from the corresponding solution peak, is observed in their EEM spectra in addition to aggregate peaks. We attribute this band to the monomeric emission, and its small red-shift may be related to planarization and rigidization of the molecules in the solid state.[24,47]

Since fluorescence emission of the thin films of **ROBDI** samples matches closely that of the corresponding crystals, we conclude that the molecular packing responsible for the luminescent properties is the same in both cases. The X-ray data demonstrate that the molecules are stacked in a cofacial manner, and the dipole moments of the neighboring stacks (AA′ and BB′) are antiparallel in **HOBDI** and **MeOBDI** and parallel in **HexOBDI** and **DdecOBDI**. In contrast to **HOBDI**, within each neighboring stack, the molecules of **MeOBDI** are slightly

translated (slipped) along the long axis and partially minimize the π-overlap between them, resulting in the highly red-shifted intense emission band. Alternatively, since the chromophore in GFP or GFP-like proteins is not consistent with a planar chromophore in the ground state[48] but freely rotating and highly twisted based on calculation,[5] it is intriguing to see if the fluorescence quenching in solid-state **HOBDI** is induced by twisting of the exo-methylene double bond in chromophore, resulting in efficient IC decay at the conical intersection.[43,49] Indeed, we have found that the angle between the phenyl and imidazole planes is the highest in the **HOBDI** derivative (7.2°, Table 2), which may correlate well with its retarded fluorescence.

The molecular packing in the single crystal of longer alkoxy chain derivatives **HexOBDI** and **DdecOBDI**, which unlike **MeOBDI** exhibit greenish-yellow and blue fluorescence, respectively, is very different. As in the other cases, the molecules of alternate stacks (AB couples) arrange in a herringbone fashion. The AB couples in **HexOBDI** and **DdecOBDI** are antiparallel molecules which are close enough to interact electronically (see Figures 9 and 10). From the crystal structure, it becomes evident that in these arrangements, the overlap between the **HexOBDI** and **DdecOBDI** chromophore parts of these structures is minimal because of the interdigitated arrangement. Instead, the main overlap occurs between the neighboring stacks (AA′ and BB′ couples). The crystal packing of **HexOBDI** and **DdecOBDI** shows that A and A′ (or B and B′) are translated along both the long and short axes relative to each other. The molecular number in each unit cell is reduced in **HexOBDI** and **DdecOBDI** as well (see Table 2). As a result of these factors, electronic interactions between the two molecules are minimized and excitonic coupling is weak. The interaction of the neighboring molecules in **DdecOBDI** is relatively weak compared to that in **HexOBDI**, resulting in dominating monomer-like blue fluorescence. Conversely, analysis of the weak interactions in the crystal structure of **HexOBDI** indicates the presence of both the monomer and red-shifted aggregate emission. It is very interesting to note that, despite the different crystal structure of all four molecules, the spectral maxima of their monomer and aggregate emissions are very close, demonstrating a weak dependence of the excitonic coupling on the nature of packing. Weakening of the intermolecular coupling in the order OH−C1−C6−C12 corresponds well with the fluorescence lifetime increase of the aggregate emission at 570 nm. Also, kinetic analysis of the monomer emission at 450 nm (Figures 5 and 6, Table 1) reveals the nature of the blue emission in **DdecOBDI** vs the yellow-green emission in **HexOBDI**. While the monomer lifetimes were the same for both species, the tailing of the aggregate emission in the low-wavelength spectral area was much larger for **DdecOBDI**. This phenomenon, and not the enhanced monomer emission, caused the hypsochromic shift of the apparent emission from **DdecOBDI** crystals. In summary, we have demonstrated that the color tuning in **ROBDI** crystals by the alkyl size variation is regulated by the monomer-aggregate emission ratio. One might conclude that these existing molecular interactions in solid state are different from those in the native β-barrel-isolated chromophore. However, by extending the alkyl chain in **ROBDI** derivatives, the emission spectrum of **DdecOBDI** becomes similar to that of the isolated, rigid GFP chromophore. Thus, isolation of the chromophore by effective control of packing by the alkyl group returns its emission to that of the protein.

Conclusion

Fluorescence "turn-on" occurs in the solid state for synthetic analogues of green fluorescence protein which are almost completely nonfluorescent in solutions. 3D steady-state and time-resolved emission spectroscopies, as well as X-ray measurements, reveal the nature of complex emission in the crystals, including the fluorescence of monomers and aggregates. The size of *O*-alkyl substituents plays a dramatic role in color tuning of crystalline luminescence. With the increase of alkyl group from methyl to hexyl to dodecyl, the interaction between the aromatic molecules in the lattice becomes weaker, resulting in a hypsochromic shift in the apparent emission from the crystals. No emission was observed from the hydroxy derivative, probably due to efficient intermolecular proton transfer. Therefore, the fluorescence of the GFP chromophores is not easily reducible to simple questions of flexibility around the benzylidene bond but rather is finely tuned by the subtle balance among intermolecular forces. We would like to point out that our observations are not limited only to the GFP, its mutants, and synthetic chromophores. An application of the GFP fluorophores as model compounds that are quenched due to free intramolecular rotation in solutions and are bright in the solid state could be extrapolated to a much wider class of organic fluorophores. Our work demonstrates an easy way of tuning their emission.

Acknowledgment. We thank the U.S. National Science Foundation (CHE-0456892 and 0809179 to L.M.T. and K.M.S.) for generous financial support. The authors thank Dr. Veaceslav Coropceanu for fruitful discussions.

Supporting Information Available: Crystallographic CIF files, details of synthesis, and analytical and spectral characterization data of compounds. This material is available free of charge via the Internet at http://pubs.acs.org.

JA806962E

(44) Davis, R.; Rath, N. P.; Das, S. *Chem. Commun.* **2004**, 74–75.
(45) (a) Kummer, A. D.; Wiehler, J.; Rehaber, H.; Kompa, C.; Steipe, B.; Michel-Beyerle, M. E. *J. Phys. Chem. B* **2000**, *104*, 4791–4798. (b) Suto, K.; Takenaka, H.; Takenaka, Y. Patent WO 2007086473. (c) Kikuchi, A.; Fukumura, E.; Karasawa, S.; Mizuno, H.; Miyawaki, A.; Shiro, Y. *Biochemistry* **2008**, *47*, 11573–11580. (d) Ai, H.-W.; Hazelwood, K. L.; Davidson, M. W.; Campbell, R. E. *Nat. Methods* **2008**, *5*, 401–403.
(46) (a) Ormö, M.; Cubitt, A. B.; Kallio, K.; Gross, L. A.; Tsien, R. Y.; Remington, S. J. *Science* **1996**, *273*, 1392–1395. (b) Wachter, R. M.; Elsliger, M. A.; Kallio, K.; Hanson, G. T.; Remington, S. J. *Structure* **1998**, *6*, 1267–1277. (c) Griesbeck, O.; Baird, G. S.; Campbell, R. E.; Zacharias, D. A.; Tsien, R. Y. *J. Biol. Chem.* **2001**, *276*, 29188–29194. (d) Rekas, A.; Alattia, J.-R.; Nagai, T.; Miyawaki, A.; Ikura, M. *J. Biol. Chem.* **2002**, *277*, 50573–50578. (e) Nagai, T.; Yamada, S.; Tominaga, T.; Ichikawa, M.; Miyawaki, A. *Proc. Natl. Acad. Sci. U.S.A.* **2004**, *101*, 10554–10559.
(47) (a) Da Como, E.; Loi, M. A.; Murgia, M.; Zamboni, R.; Muccini, M. *J. Am. Chem. Soc.* **2006**, *128*, 4277–4281. (b) Nijegorodov, N.; Zvolinsky, V.; Luhanga, P. V. C. *J. Photochem. Photobiol. A* **2008**, *196*, 219–226. (c) Chang, M.-H.; Hoffmann, M.; Anderson, H. L.; Herz, L. M. *J. Am. Chem. Soc.* **2008**, *130*, 10171–10178.
(48) Yang, F.; Moss, L.; Phillips, G. *Nat. Biotechnol.* **1996**, *14*, 1246–1251.
(49) Toniolo, A.; Olsen, S.; Manohar, L.; Martinez, T. J. *Faraday Discuss.* **2004**, *127*, 149–163.